

Lawrence Berkeley National Laboratory

LBL Publications

Title

Correlative Cryogenic Spectromicroscopy to Investigate Selenium Bioreduction Products

Permalink

<https://escholarship.org/uc/item/93c361st>

Journal

ENVIRONMENTAL SCIENCE & TECHNOLOGY, 52(2)

ISSN

0013-936X

Authors

Fakra, Shine C
Luef, Birgit
Castelle, Cindy J
[et al.](#)

Publication Date

2018

DOI

10.1021/acs.est.5b01409

Peer reviewed

1 **Correlative cryogenic spectro-microscopy to investigate**

2 **Selenium bioreduction products**

3
4 Sirine C. Fakra^{1,2*}, Birgit Luef^{1#}, Cindy J. Castelle¹, Sean W. Mullin^{1δ}, Kenneth H.
5 Williams³, Matthew A. Marcus², Denise Schichnes⁴, and Jillian F. Banfield^{1,3}

6
7 ¹*Department of Earth and Planetary Science, University of California Berkeley, Berkeley CA*
8 *94720, USA.*

9 ²*Advanced Light Source, Lawrence Berkeley National Lab, Berkeley, CA 94720, USA.*

10 ³*Earth Sciences Division, Lawrence Berkeley National Lab, Berkeley, CA 94720, USA.*

11 ⁴*Department of Plant & Microbial Biology, University of California Berkeley, Berkeley CA*
12 *94720, USA.*

13 *Corresponding author: sfakra@berkeley.edu, ph: 510-495-2855, fax: 510-486-4102.

14
15 #Current address: Department of Biotechnology, Norwegian University of Science and
16 Technology, Trondheim 7491, Norway. ^δCurrent address: Division of Geological and Planetary
17 Sciences, California Institute of Technology, Pasadena, CA 91125.

18 Submitted to: Environmental Science and Technology.

19

20 **Abstract**

21 Accurate mapping of the composition and structure of minerals and associated biological
22 materials is critical in geomicrobiology and environmental research. Here we developed an
23 apparatus allowing correlation of cryogenic transmission electron microscopy (TEM) and
24 synchrotron hard X-ray microprobe (SHXM) datasets to precisely determine the distribution,
25 valence state and structure of selenium in biofilms sampled from a contaminated aquifer near
26 Rifle, CO, USA. Results were replicated in the laboratory via anaerobic selenate-reducing
27 enrichment cultures. 16S rRNA analyses of field-derived biofilm indicated the dominance of
28 Betaproteobacteria from the Comamonadaceae family, and uncultivated members of the
29 *Simplicispira* genus. The major product in field and culture-derived biofilms is ~25-300 nm red
30 amorphous Se⁰ aggregates of colloidal nanoparticles. Correlative analyses of the cultures
31 provided direct evidence for microbial dissimilatory reduction of Se(VI) to Se(IV) to Se⁰.
32 Extended X-ray absorption fine structure spectroscopy showed red amorphous Se⁰ with a first
33 shell Se-Se interatomic distance of 2.339 ± 0.003 Å. Complementary scanning transmission X-
34 ray microscopy revealed that these aggregates are strongly associated with a protein-rich biofilm
35 matrix. These findings have important implications for predicting the stability and mobility of Se
36 bioremediation products and understanding of Se biogeochemical cycling. The approach,
37 involving correlation of cryo-SHXM and cryo-TEM datasets from the same specimen area, is
38 broadly applicable to biological and environmental samples.

39 **Introduction**

40

41 Deciphering the roles of microbial processes in biogeochemical transformations is
42 important for many bio-mineral systems and environmental research in general. Characterization
43 of field samples is necessary because relevant pure cultures or characterized mixed microbial
44 communities can be difficult to obtain, and can miss critical aspects that are key to
45 environmental processes. Damage to biological materials can occur by shrinkage, breakage or
46 loss of subcellular and extracellular structures. Furthermore, examination of dry or freeze-dried
47 samples can lead to denaturation of proteins, alteration of the mineral structure and loss of spatial
48 resolution at the cell surface-nanoparticle interface, yielding incorrect interpretations¹.

49 Most bio-mineral samples are complex, of variable chemical composition at the nano-
50 and micro-scales, and often contain poorly-ordered materials in low concentration. Synchrotron
51 hard X-ray microprobes (SHXM) are ideally suited to characterize such systems, and provide
52 metal distribution through X-ray fluorescence mapping (μ XRF), valence state, local atomic
53 structure via X-ray absorption spectroscopy (μ XAS) and phase by X-ray diffraction (μ XRD)².
54 X-ray damage through metal photo-reduction/oxidation and amorphization has been well
55 documented and is especially acute in organics-containing samples³⁻⁵. Selenium (Se) compounds
56 in particular are prone to X-ray damage as illustrated by the breaking of the C γ —Se bond in
57 selenomethionine (SeMet)⁶, selenate photoreduction⁷ and selenite photo-oxidation⁸ or just simply
58 reported such as in the case of Se-contaminated biological wastewater samples⁹. Additionally,
59 organic-bound metals and low-Z containing molecules are often difficult to analyze at room
60 temperature because thermal vibrations damp the amplitude of extended X-ray absorption fine
61 structure (EXAFS) oscillations, especially at high photo-electron wavenumbers. These issues are
62 exacerbated in dilute and/or poorly ordered bio-minerals where longer beam exposure is usually

63 required for adequate signal-to-noise ratios. To alleviate these effects, measurements are most
64 often carried out at LN₂ (77 K) or less frequently at LHe (4 K) temperatures. In the case of
65 selenium, prior Se K-edge cryo-EXAFS studies of amorphous and crystalline Se¹⁰ demonstrated
66 that the Debye-Waller thermal disorder component is only marginally reduced below 100 K,
67 suggesting that the use of LHe (versus LN₂) would not significantly improve the EXAFS signal.
68 Lastly, cryogenic analyses should allow better detection of any potentially volatile selenides
69 produced.

70 There is a strong incentive to link cryogenic SHXM with cryogenic transmission electron
71 microscopy (cryo-TEM¹¹). Cryo-TEM provides ultra-structural information at 2-4 nm
72 resolution¹². Whole frozen hydrated intact bacteria embedded in amorphous (vitreous) ice can be
73 analyzed, eliminating artifacts associated with traditional fixation and dehydration methods or
74 sectioning¹. The sample is generally cooled with LN₂ (vs. LHe¹³), and low dose imaging mode is
75 used to minimize electron damage and preserve sample structures in a “near-native” state.
76 However, cryo-TEM provides limited chemical information on thin samples (\lesssim 750 nm) within a
77 narrow field of view (100’s nm). On the other hand, SHXM is effective at characterizing, at the
78 micron scale, millimeter-scale areas of poorly concentrated samples (10’s of ppm). Ultimately
79 correlating cryo-TEM with cryo-SHXM datasets of the same sample region allows to link sub-
80 nm-scale structural information to crucial chemical speciation data. Here we use this approach to
81 investigate the distribution and speciation of selenium in biofilms from an unconfined aquifer
82 adjacent to the Colorado River, near Rifle, CO, USA. The shallow groundwater has residual
83 metal contamination (U, V, As and Se) at tens of μ M levels due to past ore-milling activities.
84 These levels exceed U.S. E.P.A. drinking water standards (100 nM for Se). To date, the potential

85 for acetate amendments into the subsurface to stimulate uranium bioreduction has been
86 extensively studied¹⁴⁻¹⁷ whereas microbiological and geochemical processes controlling selenium
87 mobility, thus toxicity at the site and others similar, are poorly understood.

88 Se occurs predominantly in four oxidation states (VI, IV, 0 and -II). Se oxyanions,
89 selenate (Se(VI), SeO_4^{2-}) and selenite (Se(IV), SeO_3^{2-}), are toxic at ppm concentrations and
90 known to bioaccumulate in the food chain causing significant ecological damage¹⁸. The
91 biogeochemical cycle of Se in nature is not well defined¹⁹ but is predominantly governed by
92 microorganisms²⁰. An important part of this cycle is the dissimilatory²¹ reduction of Se
93 oxyanions (DSeR) by anaerobes²². These microorganisms couple the oxidation of organic matter
94 (or H_2) to the reduction of Se oxyanions, forming either relatively insoluble non-toxic Se^0 or
95 reactive and toxic selenide Se(-II). Dissimilatory selenate reduction to Se^0 is a major sink for Se
96 oxyanions in anoxic environments^{22, 23}. Although phylogenetically diverse selenite-reducing
97 bacteria have been well characterized, relatively little is known about selenate-reducing bacteria.
98 On the other hand, the stability, reactivity and bioavailability of Se^0 colloids are still not well
99 understood, and likely depend strongly on the size, morphology and allotropic form of Se. A
100 handful of studies have reported microbial reduction of Se oxyanions to Se^0 , mostly as red
101 amorphous²⁴⁻²⁸ (primarily chain structure) and red crystalline monoclinic²⁹ (Se_8 rings).
102 However, few provide direct evidence of the structure of the Se allotropes produced, especially
103 from field-preserved samples.

104 Previously at the Rifle site, microbial reduction of Se oxyanions was detected during a
105 biostimulation experiment³⁰, but many questions remained about the form(s) and distribution of
106 the products. Here we developed a cryo-stage that allows the transfer of cryogenically preserved

107 Se-rich biofilms between a TEM and a SHXM, enabling essentially artifact-free ultra-structural
108 biological and chemical information from the same sample region. We used this approach to
109 examine in detail the spatial distribution and chemical speciation of selenium in samples
110 obtained through field experimentation at the Rifle site and cultivation.

111

112 **Materials and Methods**

113 Additional materials and methods can be found in the Supporting Information.

114 **Biofilm samples from the Rifle site.** The samples were collected during the “Super 8”
115 uranium bio-stimulation field experiment¹⁷ (August-September 2010) at the Rifle Integrated
116 Field Research Challenge site adjacent to the Colorado River (Western Colorado, USA). The site
117 is located on a relatively low-lying alluvial terrace created by a floodplain meander of the
118 Colorado River and is described extensively elsewhere^{14, 16}. The shallow, unconfined aquifer
119 consists of alluvial sands, silts, and gravels; details on the geochemistry and mineralogy can be
120 found in prior studies^{15, 16}. As previously described¹⁷, the groundwater was amended with sodium
121 acetate and injected into the subsurface at various depths. Acetate (CH_3COO^-) served as a carbon
122 source and electron donor over the course of the 25-day amendment period. Biofilm samples
123 were collected at well CG02 (4 m depth, 5 mM acetate), close to the down-gradient reference
124 well CD01, 16 days after injection of acetate to the anoxic aquifer. For all analyses except
125 confocal laser scanning microscopy, samples were collected by scraping the biofilm off the
126 injection tubing (polyethylene, HDPE) used to circulate the acetate-amended groundwater
127 (pH~7.2). The biofilms were uniformly distributed across the tubing, with minimal O_2 (from

128 diffusion across the tubing wall) and low nitrate level (~10 μM average). Samples were flash-
129 frozen directly in the field, to preserve their physical and chemical integrity, using a portable
130 cryo-plunger³¹ and procedures described in the Supporting Information.

131 **Enrichment cultures.** For enrichment cultivation, we sampled pieces of the tubing used
132 to deliver acetate to the subsurface, in which a biofilm had grown onto the inner surface and
133 preserved these pieces at -80 °C. Some pieces of biofilm were used for PCR amplification of
134 16S rRNA gene sequencing (see details in Supporting Information). Other pieces of biofilm were
135 thawed and added anaerobically to fresh medium in a glove box. Cultures were established
136 either in 10 mL carbonate-buffered freshwater medium (sulfate and nitrate free) or in
137 groundwater artificial medium (GWA, contains sulfate) and inoculated with sodium selenate or
138 sodium selenite (5 mM, Sigma Aldrich) and sodium acetate or sodium L- lactate (10 mM, Sigma
139 Aldrich). Details regarding the growth media can be found in the Supporting Information (Table
140 S1). Cultures were sparged with $\text{N}_2:\text{CO}_2$ (80:20) to remove dissolved oxygen and sealed with
141 butyl rubber stoppers and aluminum crimp seals, as previously described³². All cultures were
142 incubated at room temperature in the dark. Only cultures grown anaerobically using acetate as
143 the carbon source and electron donor and selenate as the sole electron acceptor were further
144 analyzed. Red precipitates were observed after 5 days, suggesting selenate reduction to Se^0 .
145 Samples were flash-frozen in the lab at various time points then stored in LN_2 until analyses.

146 **2D cryo-TEM** Cryo-TEM images were acquired with a JEOL-3100-FFC electron
147 microscope (JEOL Ltd, Akishima, Tokyo, Japan) equipped with a FEG electron source operating
148 at 300 kV, an Omega energy filter (JEOL), an LN_2 -cooled sample transfer stage (80 K), and a
149 Gatan 795 4K \times 4K CCD camera (Gatan Inc., Pleasanton, CA, USA) mounted at the exit of an

150 electron decelerator held at a voltage of 200 to 250 kV. Survey of the grids and selection of
151 suitable targets were performed in low dose defocused diffraction mode. Images were recorded
152 at different magnifications with a pixel size of 0.56 and 0.701 nm at the specimen. Several
153 images were recorded with a 2K×2K CCD camera instead, with a pixel size of 0.69, 0.92 and 1.2
154 nm at the specimen. Underfocus values ranged from $12 \pm 0.5 \mu\text{m}$ to $15 \pm 0.5 \mu\text{m}$, and energy filter
155 widths were typically around 30 eV. Over 100 images of field samples and 70 images of culture
156 samples were recorded to evaluate the morphology and size of cells and colloidal particles.

157 **X-ray microprobe.** Micro-focused X-ray fluorescence (μXRF) mapping, X-ray
158 diffraction (μXRD) and Se K-edge X-ray absorption spectroscopy data were collected at the
159 Advanced Light Source (ALS) bending magnet beamline 10.3.2 (2.4- 17 keV) with the storage
160 ring operating at 500 mA and 1.9 GeV³³. All data were recorded at 95 K using a cryo-stage
161 described below. Maps and μXRF spectra were collected at 13 keV with a beam spot size
162 ranging from $2 \times 2 \mu\text{m}$ to $5 \times 5 \mu\text{m}$, and counting times up to 200 ms/pixel. Fluorescence emission
163 counts were recorded using a seven-element Ge solid-state detector (Canberra) and XIA
164 electronics. Se K-edge μXANES spectra were recorded in fluorescence mode by continuously
165 scanning the Si (111) monochromator (Quick XAS mode) from 160 eV below up to 407 eV
166 above the edge (12500-13067 eV, i.e. up to $k = 10 \text{ \AA}^{-1}$). EXAFS spectra were recorded up to 740
167 eV above the edge (12500-13400 eV, i.e. up to $k \sim 13.7 \text{ \AA}^{-1}$). Spectra were calibrated using the
168 white line of a red amorphous Se standard set at 12660 eV. All data were processed using
169 LabVIEW custom software and standard procedures described elsewhere³⁴. To rapidly survey
170 the valence state of selenium in the samples, valence state scatter plots were generated from
171 XANES data using a spectral database of Se compounds (see **Table S2** and Supporting

172 Information). Further, least-squares linear combination fitting of the XANES spectra was
173 performed as previously described³⁵. Micro-EXAFS spectra of cultures were reduced with
174 $k^2\chi(k)$ weighting, out to $k = 12 \text{ \AA}^{-1}$ and analyzed via shell-by-shell fitting using the FEFF61
175 code and the Artemis software^{36,37}. Only the first shell was fitted, as other shells were not visible
176 enough for accurate analysis. The structure of trigonal Se^0 as described by Keller and
177 coworkers³⁸ was used to create FEFF61 input files from which to extract Se-Se paths out to 3.5 \AA
178 and fit the experimental *t*-Se EXAFS spectrum at 95 K. Fit of the culture data were performed in
179 q space (2-12 \AA) using a Kaiser-Bessel window (1.4-2.5 \AA). Details on μXRD analyses can be
180 found in the Supporting Information.

181 **Correlative cryogenic SHXM and TEM.** A custom X-ray microprobe cryo-stage (-190
182 to +150 °C, $\pm 0.1^\circ\text{C}$ precision) was designed and built in collaboration with Instec Inc, to fit the
183 geometry of the beamline and allow cryo-transfer of flash-frozen samples (**Figures 1** and **S1**).
184 The apparatus allows cryo-XRF/XAS measurements to be performed in fluorescence and/or
185 transmission modes. XRD measurements in transmission, are used to check for ice
186 contamination and quality of the transfer. The apparatus consists of four parts: a stage
187 (CLM77K), a sample loading frame (SLF) that can accommodate two round sample grid boxes,
188 a grid holder tongue (GHT) and a temperature controller (mk1000). Prior to any cold
189 experiment, the CLM77K stage is heated to +110°C for 5 minutes then purged with dry N_2 gas to
190 remove any moisture trapped. The CLM77K is cooled to -190 °C (83 K) using a pressurized LN_2
191 tank. During cooling, the sample chamber and all windows are purged with dry N_2 gas to prevent
192 water vapor condensation and frost. The SLF, placed in a LN_2 bath in a Styrofoam container, is
193 used to support the GHT during sample loading/unloading. Using the SLF, a single cryo-TEM

194 grid (or Si₃N₄ window), mounted in a JEOL 3100 TEM cartridge, can be loaded onto the GHT
195 for correlative analyses. Alternatively, another GHT designed to accommodate up to three TEM
196 grids (or windows) can also be used. In either configuration, the spring loaded GHT cover snaps
197 closed over the cryo-TEM grids, keeping them thermally insulated. Once the CLM77K is cooled
198 and stable at $-190 \pm 0.1^\circ\text{C}$, the GHT containing the cryo-samples, is then quickly inserted and
199 locked into the CLM77K, where the sample temperature reaches 95 K. Thermocouples located in
200 the GHT and CLM77K, and connected to the mk1000 are used to continuously monitor (every
201 second) the temperature of the sample and the stage respectively. Once the cryo-microprobe
202 measurements (~12 h maximum duration) are complete, the GHT with samples is cryo-
203 transferred back to the SLF in an LN₂ bath and samples are subsequently stored in LN₂.

204

205 **Results and discussion**

206 **Geochemistry**

207 Biofilm samples (referred as ‘biofilm CG02’) were collected 16 days after the start of
208 acetate amendment in the subsurface, during the Fe(III) reduction period³⁹. Acetate injection into
209 the aquifer resulted in a rapid decrease of soluble Se; the minimum concentration was reached
210 after 7 days (**Figure S2**). The concentration of dissolved Se (Se oxyanions) just prior to acetate
211 injection on day 1 was 0.81 μM, versus 0.03 μM on day 15 (closest time point to sample
212 collection), suggesting that ~96% of dissolved Se was converted into a solid phase. Soluble Se
213 concentration remained well below the U.S. EPA limit for Se in drinking water (0.1μM) past
214 biostimulation experiment. Sulfate concentrations remained stable indicating minimal sulfate
215 reduction and sulfide production during the sampling period. These trends are consistent with

216 prior acetate biostimulation experiments¹⁶ on un-amended portions of the Rifle aquifer as was
217 the case here.

218 **Microbial community composition**

219 Phylogenetic analyses of the 16S rRNA gene sequences recovered from biofilm CG02
220 show an abundance of organisms from the Betaproteobacteria class (72% of the community
221 sequences, **Figures S3 and S4**). These bacteria are often found dominant in freshwaters and
222 inferred to play an important role in the nitrogen cycle, including nitrate respiration.
223 Comamonadaceae is the most abundant family (**Figure S3C**) and uncultivated members of the
224 *Simplicispira* genus were the most abundant identified organisms (**Figures S3D and S4B**). It is
225 well known from prior studies at this site that acetate enriches for members of the
226 Comamonadaceae family, specifically the *Simplicispira*⁴⁰ genus. In fact, this result was shown
227 previously in well CD01, the same groundwater reference well used in the current study⁴¹. The
228 facultative anaerobe *Simplicispira* strain BDI⁴² (motile, weakly-curved rod) a nitrate and
229 vanadate reducer, was isolated from this site. We tested this isolate for selenate or selenite
230 reduction to Se⁰. The organism was cultivated both in nitrate-free and nitrate-amended (2 mM)
231 bicarbonate freshwater medium inoculated with acetate (5, 10 mM) and selenate (5 mM) or
232 selenite (1, 2 and 5 mM). No red (or grey/black/brown) Se⁰ precipitates were formed, indicating
233 that strain BDI does not carry out this transformation in solutions containing mM concentrations
234 of these Se oxyanions. A large number of uncultivated members of the Comamonadaceae family
235 were detected, some of which could contribute to the reduction of Se oxyanions. However, we
236 could not test this hypothesis because to date only the BDI strain has been isolated from this site.
237 Some members of the Comamonadaceae family such as *Comamonas sp.* are known selenite

238 reducers⁴³. Identified genus from this family, *Hydrogenophaga sp.* (H₂-oxidizer) are rod-shaped,
239 autotrophic denitrifiers⁴⁴ that have been correlated with nitrate and selenate fluxes⁴⁵. These
240 organisms likely contribute to selenate reduction because some strains have been reported to
241 reduce selenate and selenite to dimethyl selenide (DMSe) and dimethyl diselenide (DMDS_e)⁴⁶.

242 The second most abundant family detected was Rhodocyclaceae (**Figures S3C and**
243 **S4C**), which contains many denitrifying bacteria. Among identified genera from this family, rod-
244 shaped *Zoogloea sp.* (9%), contains strains capable of denitrification⁴⁷ and of selenite reduction
245 to elemental Se⁴⁸. *Zoogloea sp.* have also been previously detected in Se-rich biofilms from
246 Rifle³⁰. *Ferribacterium sp.*⁴⁹ and *Dechloromonas* RCB form a monophyletic group (**Figure S4C**)
247 representing 5% of the bacterial community. *Dechloromonas sp.* are well-known perchlorate and
248 nitrate-reducing bacteria⁵⁰ commonly found or used to enhance selenate reduction in
249 bioreactors^{51, 52}. *Hydrogenophaga sp.*, *Zoogloea sp.* and *Dechloromonas sp.* have been
250 previously detected in Se-rich biofilms³⁰ at Rifle and have been often detected at this site over
251 the years^{30, 53-57}. Finally, bacteria from the Chloroflexi and the Bacteroidetes phyla could also
252 contribute to selenate reduction because a variety of selenate reductases have been identified in
253 the genomes of Anaerolineaceae and Bacteroidetes⁵⁸ obtained from the Rifle site
254 (<http://ggkbase.berkeley.edu/>).

255 Organisms from unidentified genera and uncultivated *Simplicispira* members account for
256 nearly three-quarters of the bacterial community. Their potential role in Se oxyanions reduction
257 is unknown and warrants further investigation. These results suggest uncultivated members of
258 the Comamonadaceae family may play an important role in Se oxyanions reduction at this
259 location.

260 Ultrastructure and carbon speciation of the field and culture samples

261 3D confocal microscopy of biofilm CG02 revealed a 2 to 12 μm thick biofilm with
262 several haystacks of self-organized cells (**Movie S1**). On the surface of the haystack, the cells
263 range in size from 0.75 to 2.7 μm (**Movie S2**). Within the core and bottom of the stack, cells are
264 similar in length, but with an oval shape. In both field and culture samples, cells exhibited a
265 Gram-negative cell wall with an inner membrane, an outer membrane and a peptidoglycan layer
266 within a periplasmic space (**Figures 2 and S5**). Cells were weakly curved rods, rod-, oval- or
267 round-shaped, with the latter only observed in biofilm CG02. Few cells exhibited an S-layer;
268 many had visible polar flagella and/or pili. Most bacteria from biofilm CG02 had pili (**Figure**
269 **S5**). Most cells contained cytoplasmic granules. STXM-derived C K-edge XANES spectra of
270 granules (**Figure S6**) exhibits a major peak at 288.4 eV, attributed to carboxyls or esters^{59, 60},
271 likely associated with polyhydroxyalkanoates (polyesters), carbon, electron and energy storage
272 polymers commonly produced by bacteria under limited nutrients. Carbon storage granules have
273 been widely reported in organisms we detected by 16S rRNA, such as *Simplicispira sp.*⁴⁰,
274 *Dechloromonas sp.*⁶¹, *Hydrogenophaga sp.*⁶² and *Zoogloea sp.*^{47, 63}. Further, a prior study⁶⁴ on
275 members of the Comamonadaceae family showed that a N-poor medium tends to stimulate the
276 production of polyhydroxyalkanoates, whereas a C-poor environment leads to the production of
277 polyphosphates. Carbon K-edge STXM data on field and culture samples (**Figures S6 and S7**)
278 showed abundant Se-rich aggregates associated with a thick protein-rich biofilm matrix
279 containing extracellular polymeric substances (EPS) rich in acidic polysaccharides with a peak at
280 288.6 eV ($\pi^*(\text{C}=\text{O})$ transition of carboxyl group in acidic polysaccharides) and in carbonates,

281 with a signature $\pi^*(C=O)$ peak at ~ 290.3 eV. In the cultures, Se^0 CNPs located near cell
282 surfaces were coated with a protein-rich organic layer (**Figure S7**).

283 **Selenium distribution and speciation in the field and culture samples**

284 In both field and culture samples, the vast majority of colloidal nanoparticles (CNPs)
285 were found as extracellular aggregates, or as few electron dense particles on cell surfaces. SEM
286 imaging and energy dispersive spectroscopy of these particles (**Figure S8**) showed Se, with
287 traces of Ca (and Si) from the background medium. The biofilm CG02 particles were about 160
288 nm \pm 70 nm in diameter while the particles in the culture grown in bicarbonate medium were a bit
289 smaller at about 130 \pm 70 nm (**Figure S9**). Only a few Se CNPs were found on each individual
290 cell surface as seen from TEM and STXM data. Se $L_{2,3}$ edges XANES spectra of CNPs
291 compared to model compounds are shown in **Figure S10** . The spectra of Se standards are
292 consistent with prior reports^{65, 66} and spectra of CNPs from field and culture samples closely
293 match that of red amorphous Se^0 . However the allotropic form of Se cannot be accurately
294 determined at these absorption edges and thus further analysis of these spectra was not pursued.

295 By contrast, most Se compounds can easily be classified by K-edge XANES, due to a
296 clear shift (2-3 eV) of the edge position ('white line') depending on Se oxidation state (**Figure**
297 **3**). This can be explained by dipole selection rules where 1s core electrons are excited into the
298 unoccupied 4p electronic states and the edge position shifts towards higher energy as the
299 oxidation state increases. Standard spectra are consistent with prior studies⁶⁷⁻⁷⁰. Twenty nine,
300 eighteen and twenty three Se-rich regions were investigated by μ XANES on biofilm CG02,
301 cultures grown in bicarbonate or GWA medium, respectively, to get enough statistics. Cultures

302 were analyzed up to 60 days after the addition of selenate and acetate to the medium to
303 determine the end products. Typical Se K-edge XANES of the CNPs from biofilm CG02 and
304 cultures grown in bicarbonate medium are displayed in **Figure 3**, and most closely resemble that
305 of red amorphous Se. Se valence plots and least-square linear combination fitting (LSQF) of the
306 XANES spectra (see methods and Supporting Information) indicate red amorphous Se⁰ is the
307 major end product in all samples (**Figure 4 and Table S3**). Attempt at fitting the data with other
308 Se⁰ compounds such as red monoclinic- α Se, black amorphous Se and grey hexagonal Se did not
309 yield good fits. These results were further confirmed by μ XRD (**Figure S11**) on field and culture
310 samples which showed no evidence for crystalline Se (either hexagonal or monoclinic). There is
311 an accumulation of selenite during selenate reduction in the culture samples that is not observed
312 in the field data, as evidenced both in the valence plot (**Figure 4**) and fitting results (**Table S3**).

313 Correlated cryogenic SHXM/ TEM analyses of a 19-day-old culture in bicarbonate
314 medium are shown in **Figure 5 and S11**. A cluster of bacteria is found associated with $\sim 100 \pm$
315 60 nm diameter Se⁰ CNPs and traces of Se(IV). Organo-selenium and inorganic selenides were
316 not detected in this region, suggesting that reduction proceeds in a two-step reaction from Se(VI)
317 to Se(IV) to Se(0). Compared to a prior study on Se-rich biofilm³⁰, correlated cryogenic SHXM/
318 TEM allows identification of the forms of selenium present on intact organisms and resolution of
319 their ultrastructure and associated minerals. Considering the low X-ray dose applied to the frozen
320 samples (see Supporting Information), photo-reduction is an unlikely explanation for the
321 formation of these compounds. The corresponding μ XRD spectrum (**Figure S11B**) does not
322 show a match to crystalline Se⁰ (either hexagonal or monoclinic). Furthermore, we compared
323 EXAFS spectra of Se⁰ CNPs from biofilm CG02 and bicarbonate cultures (**Figure 6, Table S4**)

324 with the crystal structure of hexagonal Se^0 , as determined by Keller et al.³⁸ The 1st shell (Se-Se
325 bond) lies at $2.355 \pm 0.003 \text{ \AA}$ for the biofilm CG02 and at $2.339 \pm 0.003 \text{ \AA}$ for the bicarbonate
326 culture, respectively. These inter-atomic distances are shorter than the bond length in hexagonal
327 Se (2.374 \AA) and are consistent with previous reports for amorphous $\text{Se}^{71,72}$. Only the first shell
328 could be fitted by a shell-by-shell method, the 2nd shell was not sufficiently visible to fit due to
329 lack of structural order, thus the Se-Se-Se bond angle could not be determined. The coordination
330 numbers (N) and sigma square (σ^2) values of the samples are very similar. The biofilm CG02
331 exhibits the longest bond length among the two samples reflecting a less disordered structure.

332 Although a vast majority of the data indicated red amorphous Se^0 , a few regions analyzed
333 outside thick biofilm regions in the 19-day-old culture show crystallization, as evidenced by
334 diffraction contrast and the presence of planar defects, likely twin planes (**Figure S12**). It is
335 interesting that crystallization occurred over just 19 days at $25 \text{ }^\circ\text{C}$, given that transformation of
336 bulk red amorphous Se to grey trigonal Se should occur at appreciable rates only above $\sim 50 \text{ }^\circ\text{C}^{73}$.
337 Nonetheless, in both cultures and field samples red amorphous Se was stable for months.

338 **Dissimilatory and assimilatory selenate reducers**

339 Cryo-spectromicroscopy and 16S rRNA gene sequence analysis of field and culture
340 samples suggest the presence of DSeR organisms. In that process, selenate used as the sole
341 terminal electron acceptor is sequentially reduced to selenite and Se^0 and further to selenide. Our
342 cultivation conditions involved high selenate concentration and resulted in significant production
343 of red amorphous Se ($\sim 30\%$ of the volume). Dissimilatory reduction of selenate and selenite by
344 anaerobic bacteria generally produces abundant extracellular Se^0 particles²⁹, consistent with our

345 observations. Selenite is a known intermediate in the microbial dissimilatory reduction of
346 selenate, being produced and reduced concomitantly. By contrast, the assimilatory microbial
347 reduction of selenate does not produce selenite²⁰ but leads to the formation of organoselenium
348 and selenides, both found as minor components in our samples. Selenite can be dissimilatory
349 reduced to Se⁰ and further to selenide (e.g. H₂Se) or it can be assimilatory reduced to
350 organoselenium (e.g., SeMet) and volatile selenides (e.g. DMSe)⁷⁴

351 The presence of organic Se in our samples could be attributed to either cell lysis,
352 selenate-tolerant bacteria or potentially selenite to selenide reducing bacteria. Selenate reduction
353 is mediated by either a soluble periplasmic selenate reductase (SerABC) or a nitrate reductase or
354 via a dissimilatory sulfate-reducing pathway. A wide variety of selenate reductases have been
355 identified in the genomes of bacteria from the Rifle site (<http://ggkbase.berkeley.edu/>). Selenite
356 is usually imported into the cytoplasm where it is reduced to Se⁰ via a membrane-associated
357 reductase, followed by rapid expulsion of Se particles via a membrane efflux pump⁷⁵. Selenite is
358 reduced by reacting with proteins in a “Painter-type” reaction, suggested as a general microbial
359 detoxification reaction to Se oxyanions⁷⁶.

360 When using sulfate-containing media (GWA), some sulfate-reducing anaerobes could
361 also be capable of reducing μM amounts of selenate, although they generally do not couple this
362 reduction to growth^{28, 77}. Moreover, the ability of sulfate respirers to reduce selenate (or selenite)
363 is greatly constrained by the availability of sulfate. Se oxyanions are thermodynamically
364 predicted to be reduced prior to sulfate²² according to their respective redox potentials (+0.44 V
365 for SeO₄²⁻/SeO₃²⁻, +0.21 V for SeO₃²⁻/Se⁰, -0.22 V for SO₄²⁻/H₂S and -0.52 V for SO₄²⁻/SO₃²⁻). At
366 the shallow depth (4 meters) where biofilms were collected, the sulfate concentration (8 mM,

367 **Figure S2**) is at a level that usually precludes selenate reduction by sulfate reducers^{21, 77}. By
368 contrast, DSeR microorganisms can reduce mM amounts of selenate to Se^0 , consistent with our
369 observations. In part due to similar potentials for the $\text{SeO}_4^{2-}/\text{SeO}_3^{2-}$ (+0.44 V) and $\text{NO}_3^-/\text{NO}_2^-$
370 (+0.42 V) redox couples, microbial reduction of nitrate and selenate often occur close together⁷⁸,
371 ⁷⁹, consistent with the presence of denitrifying bacteria we find by 16S rRNA gene sequencing
372 analyses.

373 **Accumulation of selenite in cultures**

374 The accumulation of selenite observed during growth on selenate, regardless of the
375 medium used, could occur because the microbial community reduces selenate faster than
376 selenite. Alternatively, Se oxidizers may re-oxidize Se^0 to selenite. The first hypothesis is the
377 most likely, as reduction of selenite to red Se^0 by the cultures was minimal, and occurred very
378 slowly (over weeks). Oxidation of Se^0 by Se-oxidizers cannot be ruled out considering the large
379 pool of unidentified organisms, however that process is generally very slow⁸⁰. More importantly
380 in our cultures, cells are under different geochemical conditions than in the field and are
381 subjected to concentrations of Se oxyanions orders of magnitude higher (5 mM versus $\sim 1 \mu\text{M}$),
382 selectively enriching for few members of the community.

383 **Association of red amorphous Se CNPs with proteins**

384 Our results show that Se^0 CNPs are strongly associated with proteins in the biofilm^{81, 82}.
385 Particles may be surface stabilized from dissolution or phase transformation when embedded in
386 the protein-rich biofilm matrix, as suggested by prior research on biogenic and synthetic Se^0
387 nanoparticles in the presence of proteins^{83, 84}. Previous studies have suggested the presence of

388 surface-associated proteins on Se^0 produced by selenite reducers⁸⁵. More generally, prior studies
389 have shown that biogenic (and synthetic) selenium nanoparticles can be associated with a
390 plenitude of high-affinity proteins^{83, 86}. Proteins, peptides, and amino acids could be released
391 after cell death⁸⁷ and scavenged by hydrophobic elemental selenium surfaces. Alternatively,
392 bacteria may also excrete Se-binding proteins²⁴. Finally, Se^0 particles found outside cells could
393 have been released through cell lysis²⁸, as we have observed in old culture samples. Any of these
394 processes would lead to extracellular aggregation of Se^0 nanoparticles, preventing entombment
395 of cells. The aggregation of Se particles likely affects selenium mobility and transport⁸⁸, as
396 evidenced by prior work showing that aggregation induced by extracellular metal-binding
397 polypeptides and proteins plays an important role in constraining the dispersion of nanoparticles
398 in the environment⁸⁹.

399 Many anthropogenic activities (e.g., agriculture, petroleum refining, mining, glass and
400 pigment manufacturing) generate Se contaminated wastewaters. Existing treatment technologies,
401 based on chemical co-precipitation or adsorption, are rather inefficient, especially for selenate,
402 and too expensive for practical industrial use. Bioremediation represents an attractive alternative
403 approach, but strongly relies on determining accurately the chemical speciation and distribution
404 of the bio-reduction products in order to be directly applicable to a diversity of anaerobic soil and
405 groundwater environments contaminated with selenium.

406 The community of Se oxyanions reducers detected here includes several genera
407 previously detected in Se-rich biofilms collected under similar conditions at the Rifle site³⁰.
408 However, the distribution patterns and allotropic form of selenium found here are clearly
409 distinct. The prior study suggested the presence of cells encrusted with red monoclinic Se^0 , but

410 using our novel correlative cryogenic spectro-microscopy apparatus, we demonstrate that the
411 main product is extracellular red amorphous Se^0 captured in a protein-rich biofilm matrix and
412 that only few particles are associated with each cell surface. Both the newly identified protein
413 coating and extensive particle aggregation are expected to reduce re-oxidation rates, thereby
414 minimizing the rapid re-release of aqueous Se to the environment.

415

416 **Acknowledgments**

417 This material is partially based upon work supported through the Lawrence Berkeley
418 National Laboratory's Sustainable Systems Scientific Focus Area. The U.S. D.O.E. Office of
419 Science, Office of Biological and Environmental Research funded the work under contracts DE-
420 SC0004733 and DE-AC02-05CH11231. Part of the equipment was funded by the LBL EFRC
421 Center for Nanoscale Control of Geologic CO_2 . We thank Paul Baker at Instec Inc. for his help
422 with the microprobe cryo-stage, Sue Spaulding for lab support, Tolek Tylizsack for support at
423 ALS beamline 11.0.2, Mary Gilles and Steve Kelly for sharing their ESEM. We are grateful to
424 D. Strawn, A. Ryser, E.A.H. Pilon-Smits and J.L. Freeman for sharing their selenium standard
425 spectra. The Advanced Light Source is supported by the Office of Basic Energy Sciences, Office
426 of Science, U.S. D.O.E. Contract No. DE-AC02-05CH11231.

427 **Supporting Information**

428 Additional experimental details, figures, and tables as referenced in the text. This
429 material is available free of charge via the Internet at <http://pubs.acs.org>.

430

431 **References**

- 432 1. Dohnalkova, A. C.; Marshall, M. J.; Arey, B. W.; Williams, K. H.; Buck, E. C.;
 433 Fredrickson, J. K., Imaging Hydrated Microbial Extracellular Polymers: Comparative Analysis
 434 by Electron Microscopy. *Appl. Environ. Microbiol.* **2011**, *77*, (4), 1254-1262.
- 435 2. Manceau A., M. A. M., N. Tamura, *Quantitative speciation of metals in soils and*
 436 *sediments. Applications of synchrotron radiation 2002*; Vol. 49.
- 437 3. Howells, M. R.; Hitchcock, A. P.; Jacobsen, C. J., Introduction: Special issue on radiation
 438 damage. *J. Electron Spectrosc. Relat. Phenom.* **2009**, *170*, (1–3), 1-3.
- 439 4. Fayard, B.; Salomé, M.; Takemoto, K.; Kihara, H.; Susini, J., Some practical
 440 considerations about the effects of radiation damage on hydrated cells imaged by X-ray
 441 fluorescence microscopy. *J. Electron Spectrosc. Relat. Phenom.* **2009**, *170*, (1–3), 19-24.
- 442 5. Cody, G. D.; Brandes, J.; Jacobsen, C.; Wirick, S., Soft X-ray induced chemical
 443 modification of polysaccharides in vascular plant cell walls. *J. Electron Spectrosc. Relat.*
 444 *Phenom.* **2009**, *170*, (1–3), 57-64.
- 445 6. Holton, J., XANES measurements of the rate of radiation damage to selenomethionine
 446 side chains. *J. Synch. Rad.* **2007**, *14*, (1), 51-72.
- 447 7. George, G. N.; Pickering, I. J.; Pushie, M. J.; Nienaber, K.; Hackett, M. J.; Ascone, I.;
 448 Hedman, B.; Hodgson, K. O.; Aitken, J. B.; Levina, A.; Glover, C.; Lay, P. A., X-ray-induced
 449 photo-chemistry and X-ray absorption spectroscopy of biological samples. *J. Synch. Rad.* **2012**,
 450 *19*, (6), 875-886.
- 451 8. Huggins, F. E.; Sanei, H., Synchrotron-radiation-induced oxidation of selenite to selenate
 452 in coal-derived fly ash. *J. Synch. Rad.* **2011**, *18*, (3), 530-533.
- 453 9. Lenz, M.; van Hullebusch, E. D.; Farges, F.; Nikitenko, S.; Corvini, P. F. X.; Lens, P. N.
 454 L., Combined Speciation Analysis by X-ray Absorption Near-Edge Structure Spectroscopy, Ion
 455 Chromatography, and Solid-Phase Microextraction Gas Chromatography–Mass Spectrometry To
 456 Evaluate Biotreatment of Concentrated Selenium Wastewaters. *Environ. Sci. Technol.* **2010**, *45*,
 457 (3), 1067-1073.
- 458 10. Kolobov, A. V.; Oyanagi, H.; Tanaka, K.; Tanaka, K., Structural study of amorphous
 459 selenium by in situ EXAFS: Observation of photoinduced bond alternation. *Phys. Rev. B* **1997**,
 460 *55*, (2), 726-734.
- 461 11. Milne, J. L. S.; Subramaniam, S., Cryo-electron tomography of bacteria: progress,
 462 challenges and future prospects. *Nat Rev Micro* **2009**, *7*, (9), 666-675.
- 463 12. Comolli, L. R.; Banfield, J. F., Inter-species interconnections in acid mine drainage
 464 microbial communities. *Frontiers in Microbiology* **2014**, *5*, 367.
- 465 13. Comolli, L. R.; Downing, K. H., Dose tolerance at helium and nitrogen temperatures for
 466 whole cell electron tomography. *Journal of Structural Biology* **2005**, *152*, (3), 149-156.
- 467 14. Anderson, R. T.; Vrionis, H. A.; Ortiz-Bernad, I.; Resch, C. T.; Long, P. E.; Dayvault, R.;
 468 Karp, K.; Marutzky, S.; Metzler, D. R.; Peacock, A.; White, D. C.; Lowe, M.; Lovley, D. R.,
 469 Stimulating the In Situ Activity of Geobacter Species To Remove Uranium from the
 470 Groundwater of a Uranium-Contaminated Aquifer. *Appl. Environ. Microbiol.* **2003**, *69*, (10),
 471 5884-5891.

- 472 15. Campbell, K. M.; Kukkadapu, R. K.; Qafoku, N. P.; Peacock, A. D.; Leshner, E.;
473 Williams, K. H.; Bargar, J. R.; Wilkins, M. J.; Figueroa, L.; Ranville, J.; Davis, J. A.; Long, P.
474 E., Geochemical, mineralogical and microbiological characteristics of sediment from a naturally
475 reduced zone in a uranium-contaminated aquifer. *Appl. Geochem.* **2012**, *27*, (8), 1499-1511.
- 476 16. Williams, K. H.; Long, P. E.; Davis, J. A.; Wilkins, M. J.; N'Guessan, A. L.; Steefel, C.
477 I.; Yang, L.; Newcomer, D.; Spane, F. A.; Kerkhof, L. J.; McGuinness, L.; Dayvault, R.; Lovley,
478 D. R., Acetate Availability and its Influence on Sustainable Bioremediation of Uranium-
479 Contaminated Groundwater. *Geomicrobiol. J.* **2011**, *28*, (5-6), 519-539.
- 480 17. Bao, C.; Wu, H.; Li, L.; Newcomer, D.; Long, P. E.; Williams, K. H., Uranium
481 Bioreduction Rates across Scales: Biogeochemical Hot Moments and Hot Spots during a
482 Biostimulation Experiment at Rifle, Colorado. *Environ. Sci. Technol.* **2014**, *48*, (17), 10116-
483 10127.
- 484 18. Santolo, O. H. M. a. G. M., Kesterson Reservoir-Past, Present, and Future: An Ecological
485 Risk Assessment. In *Selenium in the Environment*, W.T. Frankenberger, J., and S.M. Benson, Ed.
486 Marcel Dekker: 1994; pp 69-117.
- 487 19. Shrift, A., A Selenium Cycle in Nature? *Nature* **1964**, *201*, (4926), 1304-1305.
- 488 20. W.T. Frankenberger, J., and S.M. Benson, *Selenium in the environment*. Marcel Dekker,
489 Inc. ed.; Taylor & Francis: N.Y.C., N.Y., 1994.
- 490 21. Lovley, D. R., Dissimilatory Metal Reduction. *Annu. Rev. Microbiol.* **1993**, *47*, (1), 263-
491 290.
- 492 22. Oremland, R. S.; Hollibaugh, J. T.; Maest, A. S.; Presser, T. S.; Miller, L. G.; Culbertson,
493 C. W., Selenate Reduction to Elemental Selenium by Anaerobic Bacteria in Sediments and
494 Culture: Biogeochemical Significance of a Novel, Sulfate-Independent Respiration. *Appl.*
495 *Environ. Microbiol.* **1989**, *55*, (9), 2333-2343.
- 496 23. Steinberg, N. A.; Oremland, R. S., Dissimilatory Selenate Reduction Potentials in a
497 Diversity of Sediment Types. *Appl. Environ. Microbiol.* **1990**, *56*, (11), 3550-3557.
- 498 24. Debieux, C. M.; Dridge, E. J.; Mueller, C. M.; Splatt, P.; Paszkiewicz, K.; Knight, I.;
499 Florance, H.; Love, J.; Titball, R. W.; Lewis, R. J.; Richardson, D. J.; Butler, C. S., A bacterial
500 process for selenium nanosphere assembly. *Proc. Natl. Acad. Sci. U. S. A.* **2011**, *108*, (33),
501 13480-13485.
- 502 25. Hunter, W.; Manter, D., Reduction of Selenite to Elemental Red Selenium by
503 *Pseudomonas* sp. Strain CA5. *Curr Microbiol* **2009**, *58*, (5), 493-498.
- 504 26. Kessi, J.; Ramuz, M.; Wehrli, E.; Spycher, M.; Bachofen, R., Reduction of Selenite and
505 Detoxification of Elemental Selenium by the Phototrophic Bacterium *Rhodospirillum rubrum*.
506 *Appl. Environ. Microbiol.* **1999**, *65*, (11), 4734-4740.
- 507 27. Tomei, F. A.; Barton, L. L.; Lemanski, C. L.; Zocco, T. G., Reduction of selenate and
508 selenite to elemental selenium by *Wolinella succinogenes*. *Can. J. Microbiol.* **1992**, *38*, (12),
509 1328-1333.
- 510 28. Tomei, F.; Barton, L.; Lemanski, C.; Zocco, T.; Fink, N.; Sillerud, L., Transformation of
511 selenate and selenite to elemental selenium by *Desulfovibrio desulfuricans*. *J. Ind. Microbiol.*
512 **1995**, *14*, (3-4), 329-336.
- 513 29. Oremland, R. S.; Herbel, M. J.; Blum, J. S.; Langley, S.; Beveridge, T. J.; Ajayan, P. M.;
514 Sutto, T.; Ellis, A. V.; Curran, S., Structural and Spectral Features of Selenium Nanospheres
515 Produced by Se-Respiring Bacteria. *Appl. Environ. Microbiol.* **2004**, *70*, (1), 52-60.

- 516 30. Williams, K. H.; Wilkins, M. J.; N'Guessan, A. L.; Arey, B.; Dodova, E.; Dohnalkova,
517 A.; Holmes, D.; Lovley, D. R.; Long, P. E., Field evidence of selenium bioreduction in a
518 uranium-contaminated aquifer. *Environ Microbiol Rep* **2013**, *5*, (3), 444-452.
- 519 31. Comolli, L. R.; Duarte, R.; Baum, D.; Luef, B.; Downing, K. H.; Larson, D. M.;
520 Csencsits, R.; Banfield, J. F., A portable cryo-plunger for on-site intact cryogenic microscopy
521 sample preparation in natural environments. *Microsc Res Tech* **2012**, *75*, (6), 829-836.
- 522 32. Coates, J. D.; Phillips, E. J.; Lonergan, D. J.; Jenter, H.; Lovley, D. R., Isolation of
523 *Geobacter* species from diverse sedimentary environments. *Appl. Environ. Microbiol.* **1996**, *62*,
524 (5), 1531-6.
- 525 33. Marcus, M. A.; MacDowell, A. A.; Celestre, R.; Manceau, A.; Miller, T.; Padmore, H.
526 A.; Sublett, R. E., Beamline 10.3.2 at ALS: a hard X-ray microprobe for environmental and
527 materials sciences. *J. Synch. Rad.* **2004**, *11*, (3), 239-247.
- 528 34. Kelly, S. D., Hesterberg, D., & Ravel, B, Analysis of Soils and Minerals Using X-ray
529 Absorption Spectroscopy. In *Mineralogical Methods*, Drees, A. L. U. L. R., Ed. Soil Science
530 Society of America: Madison, WI, 2008; Vol. Part 5, p 367.
- 531 35. Bañuelos, G. S.; Fakra, S. C.; Walse, S. S.; Marcus, M. A.; Yang, S. I.; Pickering, I. J.;
532 Pilon-Smits, E. A. H.; Freeman, J. L., Selenium Accumulation, Distribution, and Speciation in
533 Spineless Prickly Pear Cactus: A Drought- and Salt-Tolerant, Selenium-Enriched Nutraceutical
534 Fruit Crop for Biofortified Foods. *Plant Physiol.* **2011**, *155*, (1), 315-327.
- 535 36. Newville, M., IFEFFIT: interactive XAFS analysis and FEFF fitting. *J. Synchrotron*
536 *Radiation* **2001**, *8*, (2), 322-324.
- 537 37. Ravel, B.; Newville, M., ATHENA, ARTEMIS, HEPHAESTUS: data analysis for X-ray
538 absorption spectroscopy using IFEFFIT. *J. Synchrotron Radiation* **2005**, *12*, (4), 537-541.
- 539 38. Keller, R.; Holzapfel, W. B.; Schulz, H., Effect of pressure on the atom positions in Se
540 and Te. *Phys. Rev. B* **1977**, *16*, (10), 4404-4412.
- 541 39. Luef, B.; Fakra, S. C.; Csencsits, R.; Wrighton, K. C.; Williams, K. H.; Wilkins, M. J.;
542 Downing, K. H.; Long, P. E.; Comolli, L. R.; Banfield, J. F., Iron-reducing bacteria accumulate
543 ferric oxyhydroxide nanoparticle aggregates that may support planktonic growth. *ISME J* **2013**,
544 *7*, (2), 338-350.
- 545 40. Grabovich, M.; Gavrish, E.; Kuever, J.; Lysenko, A. M.; Podkopaeva, D.; Dubinina, G.,
546 Proposal of *Giesbergeria voronezhensis* gen. nov., sp. nov. and *G. kuznetsovii* sp. nov. and
547 reclassification of [*Aquaspirillum*] *anulus*, [*A.*] *sinuosum* and [*A.*] *giesbergeri* as *Giesbergeria*
548 *anulus* comb. nov., *G. sinuosa* comb. nov. and *G. giesbergeri* comb. nov., and [*Aquaspirillum*]
549 *metamorphum* and [*A.*] *psychrophilum* as *Simplicispira metamorpha* gen. nov., comb. nov. and
550 *S. psychrophila* comb. nov. *INT J SYST EVOL MICR* **2006**, *56*, (3), 569-576.
- 551 41. Yelton, A. P.; Williams, K. H.; Fournelle, J.; Wrighton, K. C.; Handley, K. M.; Banfield,
552 J. F., Vanadate and Acetate Biostimulation of Contaminated Sediments Decreases Diversity,
553 Selects for Specific Taxa, and Decreases Aqueous V5+ Concentration. *Environ. Sci. Technol.*
554 **2013**, *47*, (12), 6500-6509.
- 555 42. Yelton, A. P. Metagenomic and Cultivation-Based Analysis of Novel Microorganisms
556 and Functions in Metal-Contaminated Environments. UC Berkeley, Berkeley, 2012.
- 557 43. Zheng, S.; Su, J.; Wang, L.; Yao, R.; Wang, D.; Deng, Y.; Wang, R.; Wang, G.; Rensing,
558 C., Selenite reduction by the obligate aerobic bacterium *Comamonas testosteroni* S44 isolated
559 from a metal-contaminated soil. *BMC microbiology* **2014**, *14*, 204.

- 560 44. Willems, A.; Busse, J.; Goor, M.; Pot, B.; Falsen, E.; Jantzen, E.; Hoste, B.; Gillis, M.;
561 Kersters, K.; Auling, G.; De Ley, J., Hydrogenophaga, a New Genus of Hydrogen-Oxidizing
562 Bacteria That Includes Hydrogenophaga flava comb. nov. (Formerly Pseudomonas flava),
563 Hydrogenophaga palleronii (Formerly Pseudomonas palleronii), Hydrogenophaga pseudoflava
564 (Formerly Pseudomonas pseudoflava and “Pseudomonas carboxydoflava”), and
565 Hydrogenophaga taeniospiralis (Formerly Pseudomonas taeniospiralis). *Int. J. Syst. Evol. Bac.*
566 **1989**, *39*, (3), 319-333.
- 567 45. Lai, C.-Y.; Yang, X.; Tang, Y.; Rittmann, B. E.; Zhao, H.-P., Nitrate Shaped the
568 Selenate-Reducing Microbial Community in a Hydrogen-Based Biofilm Reactor. *Environ. Sci.*
569 *Technol.* **2014**, *48*, (6), 3395-3402.
- 570 46. Ranjard, L.; Prigent-Combaret, C.; Favre-Bonté, S.; Monnez, C.; Nazaret, S.; Cournoyer,
571 B., Characterization of a novel selenium methyltransferase from freshwater bacteria showing
572 strong similarities with the calicheamicin methyltransferase. *BBA - Gene Structure and*
573 *Expression* **2004**, *1679*, (1), 80-85.
- 574 47. Dugan, P.; Stoner, D.; Pickrum, H., The Genus Zoogloea. In *The Prokaryotes*, Dworkin,
575 M.; Falkow, S.; Rosenberg, E.; Schleifer, K.-H.; Stackebrandt, E., Eds. Springer New York:
576 2006; pp 960-970.
- 577 48. Srivastava, N.; Mukhopadhyay, M., Biosynthesis and structural characterization of
578 selenium nanoparticles mediated by Zoogloea ramigera. *Powder Technol.* **2013**, *244*, (0), 26-29.
- 579 49. Cummings, D. E.; Caccavo Jr, F.; Spring, S.; Rosenzweig, R. F., Ferribacterium
580 limneticum, gen. nov., sp. nov., an Fe(III)-reducing microorganism isolated from mining-
581 impacted freshwater lake sediments. *Arch Microbiol* **1999**, *171*, (3), 183-188.
- 582 50. Coates, J. D.; Chakraborty, R.; Lack, J. G.; O'Connor, S. M.; Cole, K. A.; Bender, K. S.;
583 Achenbach, L. A., Anaerobic benzene oxidation coupled to nitrate reduction in pure culture by
584 two strains of Dechloromonas. *Nature* **2001**, *411*, (6841), 1039-1043.
- 585 51. Zhang, Y.; Frankenberger Jr, W. T., Supplementing Bacillus sp. RS1 with
586 Dechloromonas sp. HZ for enhancing selenate reduction in agricultural drainage water. *Sci. Total*
587 *Environ.* **2007**, *372*, (2-3), 397-405.
- 588 52. Chung, J.; Ryu, H.; Abbaszadegan, M.; Rittmann, B. E., Community structure and
589 function in a H(2)-based membrane biofilm reactor capable of bioreduction of selenate and
590 chromate. *Appl Microbiol Biotechnol* **2006**, *72*, (6), 1330-1339.
- 591 53. Mouser, P. J.; N'Guessan, A. L.; Elifantz, H.; Holmes, D. E.; Williams, K. H.; Wilkins,
592 M. J.; Long, P. E.; Lovley, D. R., Influence of Heterogeneous Ammonium Availability on
593 Bacterial Community Structure and the Expression of Nitrogen Fixation and Ammonium
594 Transporter Genes during in Situ Bioremediation of Uranium-Contaminated Groundwater.
595 *Environ. Sci. Technol.* **2009**, *43*, (12), 4386-4392.
- 596 54. N'Guessan, A. L.; Elifantz, H.; Nevin, K. P.; Mouser, P. J.; Methe, B.; Woodard, T. L.;
597 Manley, K.; Williams, K. H.; Wilkins, M. J.; Larsen, J. T.; Long, P. E.; Lovley, D. R., Molecular
598 analysis of phosphate limitation in Geobacteraceae during the bioremediation of a uranium-
599 contaminated aquifer. *ISME J* **2009**, *4*, (2), 253-266.
- 600 55. Handley, K. M.; Wrighton, K. C.; Piceno, Y. M.; Andersen, G. L.; DeSantis, T. Z.;
601 Williams, K. H.; Wilkins, M. J.; N'Guessan, A. L.; Peacock, A.; Bargar, J.; Long, P. E.; Banfield,
602 J. F., High-density PhyloChip profiling of stimulated aquifer microbial communities reveals a
603 complex response to acetate amendment. *FEMS Microbiol. Ecol.* **2012**, *81*, (1), 188-204.

- 604 56. Wrighton, K. C.; Thomas, B. C.; Sharon, I.; Miller, C. S.; Castelle, C. J.; VerBerkmoes,
605 N. C.; Wilkins, M. J.; Hettich, R. L.; Lipton, M. S.; Williams, K. H.; Long, P. E.; Banfield, J. F.,
606 Fermentation, Hydrogen, and Sulfur Metabolism in Multiple Uncultivated Bacterial Phyla.
607 *Science* **2012**, *337*, (6102), 1661-1665.
- 608 57. Wrighton, K. C.; Castelle, C. J.; Wilkins, M. J.; Hug, L. A.; Sharon, I.; Thomas, B. C.;
609 Handley, K. M.; Mullin, S. W.; Nicora, C. D.; Singh, A.; Lipton, M. S.; Long, P. E.; Williams,
610 K. H.; Banfield, J. F., Metabolic interdependencies between phylogenetically novel fermenters
611 and respiratory organisms in an unconfined aquifer. *ISME J* **2014**, *8*, (7), 1452-1463.
- 612 58. Handley, K. M.; VerBerkmoes, N. C.; Steefel, C. I.; Williams, K. H.; Sharon, I.; Miller,
613 C. S.; Frischkorn, K. R.; Chourey, K.; Thomas, B. C.; Shah, M. B.; Long, P. E.; Hettich, R. L.;
614 Banfield, J. F., Biostimulation induces syntrophic interactions that impact C, S and N cycling in
615 a sediment microbial community. *ISME J* **2013**, *7*, (4), 800-816.
- 616 59. Boyce, C. K.; Cody, G. D.; Feser, M.; Jacobsen, C.; Knoll, A. H.; Wirick, S., Organic
617 chemical differentiation within fossil plant cell walls detected with X-ray spectromicroscopy.
618 *Geology* **2002**, *30*, (11), 1039-1042.
- 619 60. Cody, G. D.; Ade, H.; Wirick, S.; Mitchell, G. D.; Davis, A., Determination of chemical-
620 structural changes in vitrinite accompanying luminescence alteration using C-NEXAFS analysis.
621 *Organic Geochem.* **1998**, *28*, (7-8), 441-455.
- 622 61. Salinero, K.; Keller, K.; Feil, W.; Feil, H.; Trong, S.; Di Bartolo, G.; Lapidus, A.,
623 Metabolic analysis of the soil microbe *Dechloromonas aromatica* str. RCB: indications of a
624 surprisingly complex life-style and cryptic anaerobic pathways for aromatic degradation. *BMC*
625 *Genomics* **2009**, *10*, (1), 351.
- 626 62. Yoon, S. C.; Choi, M. H., Local Sequence Dependence of Polyhydroxyalkanoic Acid
627 Degradation in *Hydrogenophaga pseudoflava*. *J. Biol. Chem.* **1999**, *274*, (53), 37800-37808.
- 628 63. Saito, T.; Saegusa, H.; Miyata, Y.; Fukui, T., Intracellular degradation of poly(3-
629 hydroxybutyrate) granules of *Zoogloea ramigera* I-16-M. *FEMS Microbiol. Lett.* **1992**, *103*, (2-
630 4), 333-338.
- 631 64. Spring, S.; Wagner, M.; Schumann, P.; Kämpfer, P., *Malikia granosa* gen. nov., sp. nov.,
632 a novel polyhydroxyalkanoate- and polyphosphate-accumulating bacterium isolated from
633 activated sludge, and reclassification of *Pseudomonas spinosa* as *Malikia spinosa* comb. nov. *Int.*
634 *J. Syst. Evol. Micr.* **2005**, *55*, (2), 621-629.
- 635 65. J. Madwid, R. A., R. Blyth, I. Coulthard, C.J. Doonan, D. Liu, R. Hoffmeyer, M.J.
636 Pushie, T. Regier, J. Ruzkowski, S.P. Singh, D. Thavarajah, C.I.E. Wiramanaden, S.I. Yang, L.
637 Zhang, G.N. George, I.J. Pickering *Selenium L-edge spectroscopy at the SGM Beamline as a tool*
638 *for environmental selenium speciation*; CLS: 2008.
- 639 66. Bugaris, D. E.; Copping, R.; Tyliszczak, T.; Shuh, D. K.; Ibers, J. A., La₂U₂Se₉: An
640 Ordered Lanthanide/Actinide Chalcogenide with a Novel Structure Type. *Inorg. Chem.* **2010**, *49*,
641 (5), 2568-2575.
- 642 67. Pickering, I. J.; Brown, G. E.; Tokunaga, T. K., Quantitative Speciation of Selenium in
643 Soils Using X-ray Absorption Spectroscopy. *Environmental Science & Technology* **1995**, *29*, (9),
644 2456-2459.
- 645 68. Ryser, A.; Strawn, D.; Marcus, M.; Johnson-Maynard, J.; Gunter, M.; Moller, G., Micro-
646 spectroscopic investigation of selenium-bearing minerals from the Western US Phosphate
647 Resource Area. *Geochemical Transactions* **2005**, *6*, (1), 1.

- 648 69. Ryser, A. L.; Strawn, D. G.; Marcus, M. A.; Fakra, S.; Johnson-Maynard, J. L.; Möller,
649 G., Microscopically Focused Synchrotron X-ray Investigation of Selenium Speciation in Soils
650 Developing on Reclaimed Mine Lands. *Environmental Science & Technology* **2005**, *40*, (2), 462-
651 467.
- 652 70. Sarret, G.; Avoscan, L.; Carrière, M.; Collins, R.; Geoffroy, N.; Carrot, F.; Covès, J.;
653 Gouget, B., Chemical Forms of Selenium in the Metal-Resistant Bacterium *Ralstonia*
654 *metallidurans* CH34 Exposed to Selenite and Selenate. *Applied and Environmental Microbiology*
655 **2005**, *71*, (5), 2331-2337.
- 656 71. Majid, M.; Bénazeth, S.; Souleau, C.; Purans, J., XAFS study of interchain and intrachain
657 order in Se1-xTex glasses: Nearest neighbors. *Phys. Rev. B* **1998**, *58*, (10), 6104-6114.
- 658 72. Yang, S. I.; Lawrence, J. R.; Swerhone, G. D. W.; Pickering, I. J., Biotransformation of
659 selenium and arsenic in multi-species biofilm. *Environ. Chem.* **2011**, *8*, (6), 543-551.
- 660 73. Minaev, V. S.; Timoshenkov, S. P.; Kalugin, V. V., Structural and phase transformations
661 in condensed selenium. *J Optoelectron Adv Mater.* **2005**, *7*, (4), 1717-1741.
- 662 74. Herbel, M. J.; Blum, J. S.; Oremland, R. S.; Borglin, S. E., Reduction of Elemental
663 Selenium to Selenide: Experiments with Anoxic Sediments and Bacteria that Breathe Se-
664 Oxyanions. *Geomicrobiol. J.* **2003**, *20*, (6), 587-602.
- 665 75. Losi, M. E.; Frankenberger, W. T., Reduction of Selenium Oxyanions by *Enterobacter*
666 *cloacae* SLD1a-1: Isolation and Growth of the Bacterium and Its Expulsion of Selenium
667 Particles. *Appl. Environ. Microbiol.* **1997**, *63*, (8), 3079-84.
- 668 76. Harrison, J. J.; Ceri, H.; Turner, R. J., Multimetal resistance and tolerance in microbial
669 biofilms. *Nat Rev Micro* **2007**, *5*, (12), 928-938.
- 670 77. Zehr, J. P.; Oremland, R. S., Reduction of Selenate to Selenide by Sulfate-Respiring
671 Bacteria: Experiments with Cell Suspensions and Estuarine Sediments. *Appl. Environ.*
672 *Microbiol.* **1987**, *53*, (6), 1365-1369.
- 673 78. Oremland, R. S.; Blum, J. S.; Bindi, A. B.; Dowdle, P. R.; Herbel, M.; Stolz, J. F.,
674 Simultaneous Reduction of Nitrate and Selenate by Cell Suspensions of Selenium-Respiring
675 Bacteria. *Appl. Environ. Microbiol.* **1999**, *65*, (10), 4385-4392.
- 676 79. Steinberg, N. A.; Blum, J. S.; Hochstein, L.; Oremland, R. S., Nitrate Is a Preferred
677 Electron Acceptor for Growth of Freshwater Selenate-Respiring Bacteria. *Appl. Environ.*
678 *Microbiol.* **1992**, *58*, (1), 426-428.
- 679 80. Dowdle, P. R.; Oremland, R. S., Microbial Oxidation of Elemental Selenium in Soil
680 Slurries and Bacterial Cultures. *Environ. Sci. Technol.* **1998**, *32*, (23), 3749-3755.
- 681 81. Flemming, H. C.; Wingender, J., The biofilm matrix. *Nature reviews. Microbiology* **2010**,
682 *8*, (9), 623-33.
- 683 82. Sutherland, I. W., The biofilm matrix – an immobilized but dynamic microbial
684 environment. *Trends in Microbiol.* **2001**, *9*, (5), 222-227.
- 685 83. Dobias, J.; Suvorova, E. I.; Bernier-Latmani, R., Role of proteins in controlling selenium
686 nanoparticle size. *Nanotechnology* **2011**, *22*, (19), 195605.
- 687 84. Kaur, G.; Iqbal, M.; Bakshi, M. S., Biomineralization of Fine Selenium Crystalline Rods
688 and Amorphous Spheres. *J Phys Chem C* **2009**, *113*, (31), 13670-13676.
- 689 85. Pearce, C. I.; Patrick, R. A. D.; Law, N.; Charnock, J. M.; Coker, V. S.; Fellowes, J. W.;
690 Oremland, R. S.; Lloyd, J. R., Investigating different mechanisms for biogenic selenite
691 transformations: *Geobacter sulfurreducens*, *Shewanella oneidensis* and *Veillonella atypica*. *Env.*
692 *Technol.* **2009**, *30*, (12), 1313-1326.

- 693 86. Lenz, M.; Kolvenbach, B.; Gygax, B.; Moes, S.; Corvini, P. F., Shedding light on
694 selenium biomineralization: proteins associated with bionanominerals. *Appl Environ Microbiol*
695 **2011**, *77*, (13), 4676-80.
- 696 87. Bayles, K. W., The biological role of death and lysis in biofilm development. *Nat Rev*
697 *Micro* **2007**, *5*, (9), 721-726.
- 698 88. Buchs, B.; Evangelou, M. W. H.; Winkel, L. H. E.; Lenz, M., Colloidal Properties of
699 Nanoparticulate Biogenic Selenium Govern Environmental Fate and Bioremediation
700 Effectiveness. *Environ. Sci. Technol.* **2013**, *47*, (5), 2401-2407.
- 701 89. Moreau, J. W.; Weber, P. K.; Martin, M. C.; Gilbert, B.; Hutcheon, I. D.; Banfield, J. F.,
702 Extracellular Proteins Limit the Dispersal of Biogenic Nanoparticles. *Science* **2007**, *316*, (5831),
703 1600-1603.

704

705

706

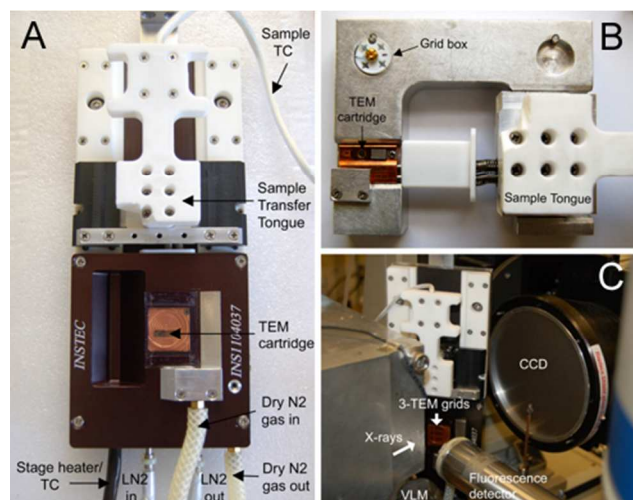


Figure 1. SHXM cryo-stage allowing correlative cryogenic TEM/microprobe measurements. A) CLM77K stage with the JEOL 3100 TEM cartridge sample transfer tongue inserted. B) View of the cartridge grid holder tongue installed on the mounting frame. C) View of the stage at beamline 10.3.2, with the sample transfer tongue inserted. The sample is oriented at 45 degrees to the incident beam, micro-XRD is performed in transmission mode.

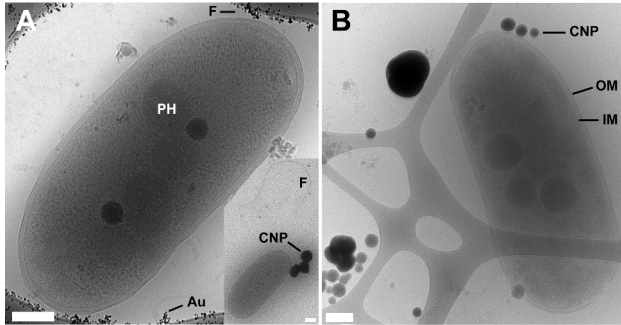


Figure 2. Cryo-TEM images of anaerobes, colloidal nanoparticles and aggregates from (A) Biofilm CG02 and (B) Selenate-reducing enrichment culture (19-day-old) grown in bicarbonate medium. IM = inner membrane, OM= outer membrane, F= flagellum, PH= polyhydroxyalkanoates, CNP= colloidal nanoparticles, Au= gold fiducial particles on a carbon coated lacy Formvar film. Scale bars are 200 nm.

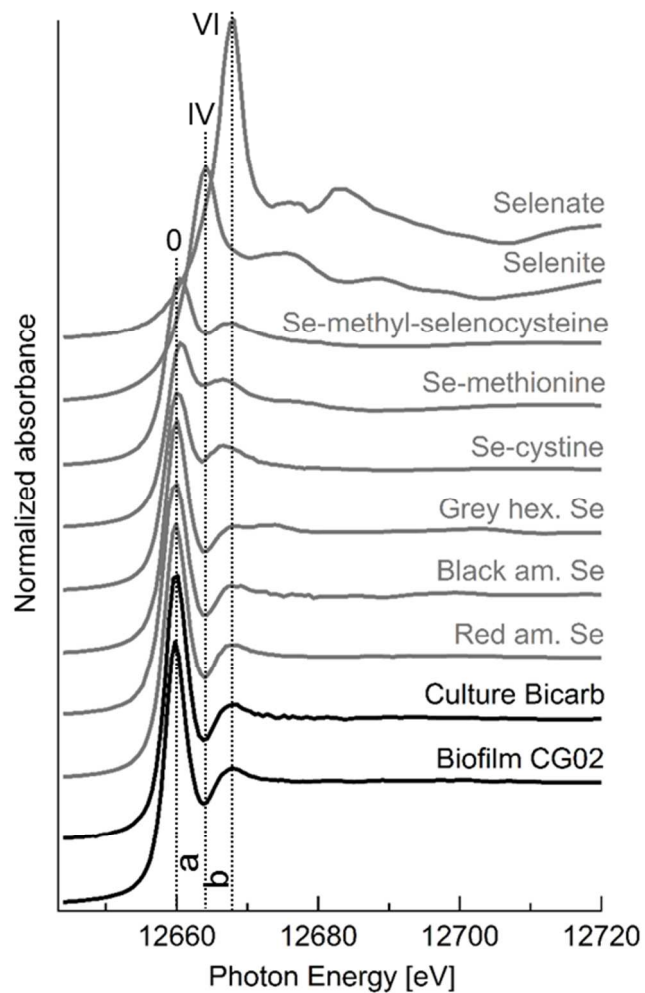


Figure 3. Se K-edge μ XANES spectra of biofilm CG02 and of a 19-day-old culture grown in bicarbonate medium, compared with a subset of standards (see **Table S2** for the complete list). Normalized XANES values at 12664.25 (IV dashed line) and 12667.8 eV (VI dashed line) were used to generate the Se valence state plot displayed in **Figure 4** (see Supporting Information).

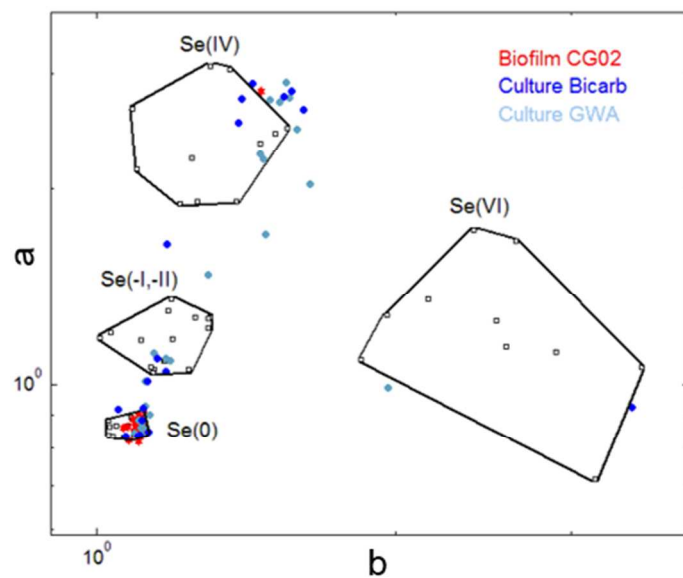


Figure 4. Se valence state scatter plot. The standards are shown in open black squares, the biofilm CG02 in red (29 spots) and the enrichment cultures grown in bicarbonate medium in dark blue (18 spots) or in groundwater artificial medium in light blue (23 spots). The Se(-II, -I) group includes organic Se compounds. See methods and Supporting Information for further details. Results of least-square linear combination fitting of all sample μ XANES spectra are summarized in **Table S3**. Both analyses indicate that Se^0 is the main product in field-derived and culture samples.

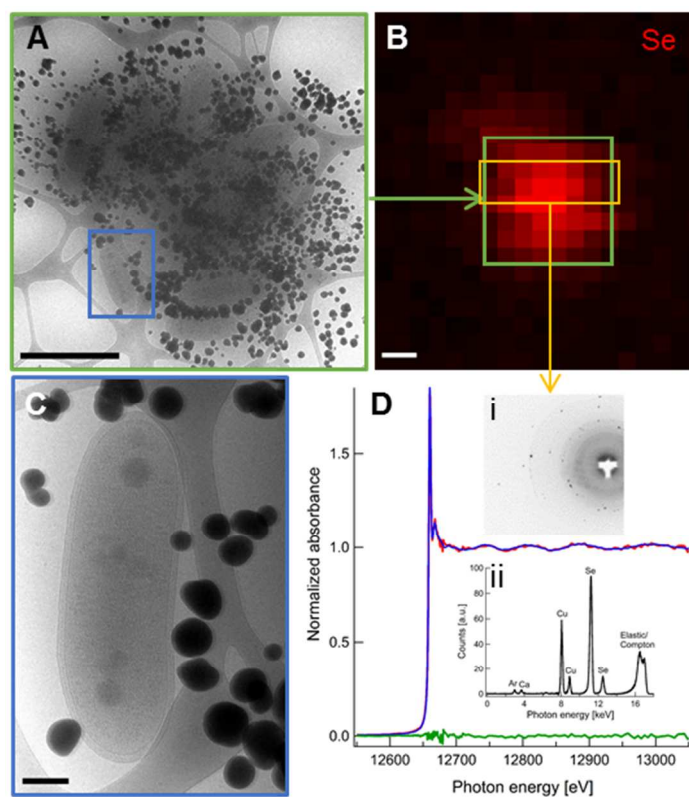


Figure 5. Correlative cryogenic spectro-microscopy on a 19-day-old culture grown in bicarbonate medium. A) Low dose cryo-TEM image (3.5 nm pixels, $7.2 \times 7.2 \mu\text{m}^2$) of a cluster of bacteria and associated Se CNP aggregates. B) Cryo- μXRF Se distribution map at 13keV (2 μm beam, 1 μm pixels). The green box area represents the entire TEM region. C) Low dose cryo-TEM image at higher magnification of the blue box area of panel A. D) Cryogenic Se K-edge μXANES (in red) collected in the orange box area of panel B. Best fit (in blue) is obtained using 87% red amorphous Se and 13% sodium selenite standards. Residual is plotted in green (normalized sum-sq is $1.25 \cdot 10^{-4}$). Insets i and ii: Cryo- μXRD pattern and - μXRF spectrum, respectively, collected at 17 keV in the orange box area. XRD showed no evidence for crystalline Se^0 (see **Figure S11**). Red amorphous Se^0 aggregates ($\sim 100 \pm 60$ nm) is the main

product of selenate reduction in this region of the sample, with minor presence of Se(IV), suggesting a 2-step reduction process. Scale bars are 2 μm (A-B) and 200 nm (C).

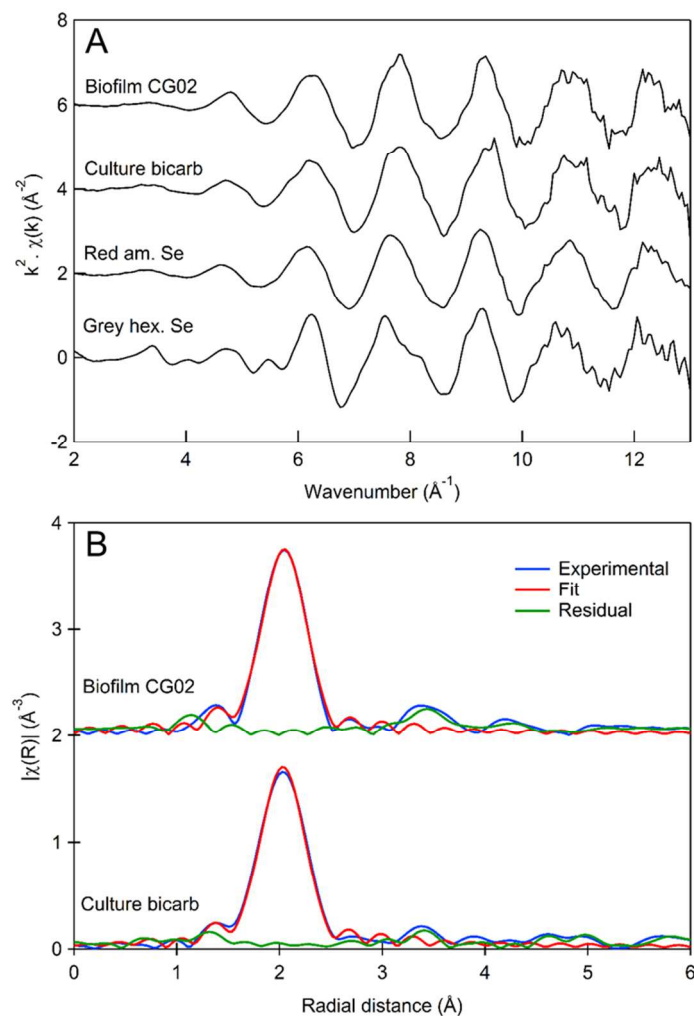


Figure 6. Cryo- μ EXAFS of biofilm CG02 and of a 19-day-old selenate-reducing enrichment culture grown in bicarbonate medium A) in k -space, compared to red amorphous Se^0 and hexagonal grey Se^0 (Se foil) standards. B) Shell-by-shell fitting analysis of the 1st shell (see Table S4) with Se-Se interatomic distance at $2.355 \pm 0.003 \text{ \AA}$ for the biofilm CG02 and $2.339 \pm 0.003 \text{ \AA}$ for the culture. Experimental spectra are shown in blue, the fits (performed in q space) in red and the residuals in green.

TOC

